Brain, Behavior, and Immunity 136 (2026) 106554

Contents lists available at ScienceDirect

Brain Behavior and Immunity

journal homepage: www.elsevier.com/locate/ybrbi

Short Communication

Immune control of sleep pressure via interferon-γ in mice

Alessandro Mormino [a,1], Federico Tucci [b,1], Germana Cocozza [a,*], Claudio Del Percio [a], Letizia Mazzarella [a], Erika Di Pietro [a], Maria Amalia Di Castro [a], Giuseppina Chece [a], Giovanni Bernardini [c], Giuseppe Sciumè [c], Giovanna Peruzzi [d], Helena Stabile [c], Cinzia Fionda [c], Mattia Laffranchi [c], Silvano Sozzani [c,e], Claudio Babiloni [a,f], Cristina Limatola [a,e,g,*,2], Stefano Garofalo [a,2]

[a] Department of Physiology and Pharmacology "V. Erspamer", Sapienza University of Rome, Rome, Italy
[b] Department of Human Neurosciences, Sapienza University of Rome, Rome, Italy
[c] Department of Molecular Medicine, Sapienza University of Rome, Rome, Italy
[d] Center for Life Nano & Neuro Science, Istituto Italiano di Tecnologia, Rome, Italy
[e] Laboratory affiliated to Istituto Pasteur, Italy
[f] IRCCS San Raffaele Roma - Cassino, Cassino Site, Cassino, Italy
[g] IRCCS Neuromed, Pozzilli, Italy

ARTICLE INFO

Keywords:
Sleep pressure
Innate Immunity
nNOS+ Interneuron
Interferon-gamma
NREM sleep

ABSTRACT

Sleep pressure reflects the brain's homeostatic need to sleep, but the mechanisms underlying its regulation remain poorly understood. In mice, a subset of cortical inhibitory neuronal nitric oxide synthase (nNOS) positive interneurons tunes the electroencephalographic slow wave activity in the delta band (<4 Hz), marker of sleep pressure. Here, we demonstrate that in mice the natural killer (NK) cells and innate lymphoid cells (ILC)1 depletion inhibits nNOS+ interneurons and EEG delta activity reducing the time spent in the non-rapid eye movement (NREM) sleep. The optogenetic re-activation of nNOS+ interneurons in the cingulate cortex of NK cell/ILC1-depleted mice rescues the EEG delta activity, confirming the link between innate immune cells-nNOS+ interneurons-sleep pressure. Finally, we demonstrated that meningeal NK/ILC1 cells produce IFN-γ in a circadian independent manner and that IFN-γ blockade *in vivo* mimics the effect of NK cell depletion in mice. These findings provide insights into the complex network involved in sleep regulation and further support the contribution of the innate immune system on sleep pressure.

1. Introduction

In mice, non-rapid eye movement (NREM) sleep following prolonged wakefulness showed ample electroencephalographic (EEG) delta activity at 0.5–4 Hz (slow-wave activity, SWA), which increased proportionally to the duration and intensity of pre-sleep activity. The amplitude of the SWA during the NREM sleep reflects the homeostatic build-up of sleep pressure over time (Huber et al., 2004; Morairty et al., 2013; Sawada et al., 2024). The greatest EEG effects occur in the most active brain regions in the last wake period (Gerashchenko et al., 2008; Thomas et al., 2020; Vyazovskiy et al., 2004) and this localized increase in EEG delta power has been linked to the poor cognitive performance and altered cortical activity observed in sleep deprived humans (Kattler et al., 1994; Siclari and Tononi, 2017).

Recent evidence demonstrated that in mice, during NREM sleep, the EEG delta power is regulated by the activation of a subset of sleep-active GABAergic interneurons that express nNOS, concentrated in layers V and VI of the cingulate cortex (Gerashchenko et al., 2018, 2008; Morairty et al., 2013; Pasumarthi et al., 2010). Indeed, the proportion of nNOS-active interneurons during NREM sleep is correlated with delta power, which directly correlates with the sleep pressure (Gerashchenko et al., 2018, 2008; Morairty et al., 2013; Pasumarthi et al., 2010). In addition, nNOS knock-out mice failed to reach a physiological delta power showing an aberrant sleep architecture (Morairty et al., 2013;

* Corresponding authors.
E-mail addresses: germana.cocozza@uniroma1.it (G. Cocozza), cristina.limatola@uniroma1.it (C. Limatola).
[1] Co-first author.
[2] Co-last author.

https://doi.org/10.1016/j.bbi.2026.106554
Received 1 October 2025; Received in revised form 28 February 2026; Accepted 22 March 2026
Available online 23 March 2026

Zielinski et al., 2019).

In the present study, we explored the interaction between the innate immune system and sleep in mice, characterizing the role of NK cells and innate lymphoid cells (ILC) 1 in regulating the delta power and the NREM sleep. We demonstrate that NK1.1 cell depletion (including ILC1, NKT cells and NK cells) reduced the time spent asleep during the light period and disrupted the NREM EEG delta activity during the dark period. These effects were mimicked by IFN-γ blockade and both NK1.1+ cell depletion and IFN-γ blockade reduced the activation of cortical nNOS+ interneurons in the cingulate cortex, modulating the EEG delta power. These findings establish NK/ILC1 cells as new components of the sleep homeostatic circuit in mice, contributing to filling the gaps to understand the immune system-sleep relationship under physiological conditions.

2. Methods

2.1. Animals

Experiments described in the present work were approved by the Animal Welfare Body of Sapienza University and the Italian Ministry of Health (authorization n° 775/2020-PR; n° 70/2022; n° 356/2023-PR) in accordance with the guidelines on the ethical use of animals from the European Community Council Directive of September 22, 2010 (2010/63/EU), and from the Italian D.Leg 26/2014. All possible efforts were made to minimize animal suffering, and to reduce the number of.

animals used per condition by calculating the necessary sample size before performing the experiments. All studies were performed using adult male mice at the indicated ages. *C57BL/6* (IgG *wild type-wt*) and nNOS^{cre} (B6.129-*Nos1*$^{tm1\ (cre)Mgmj}$/J, RRID:IMSR_JAX:017526) were obtained from Charles River (Calco, Italy) and from Jackson Laboratory (Bar Harbor, ME, USA). Mice were housed in standard breeding cages at constant temperature (22 ± 1 °C) and relative humidity (50%), with a 12:12 h light:dark cycle (light onset at 07:00 AM). Food and water were available ad libitum.

2.2. Mice treatment

Starting at 6 weeks of age, *C57BL/6J* and nNOS^{cre} mice were randomly grouped for the treatments. NK cell depletion was performed using a blocking Ab against NK1.1, which recognizes an epitope of the NKR1Pc-activating receptor (PK136). Mice were, intraperitoneally, injected with 50 μg (in 100 μl) of anti-NK1.1 Ab every 2 days the first week, every 4 days the second week and then repeated once a week until the age described in the text, at least three weeks. NK cell depletion from the blood sample and meninges was monitored by FACS (as in Garofalo et al., 2023). For Ab anti-IFNγ treatment, mice were treated with 200 μg of rat XMG1.2, by intraperitoneal injection repeated every 5 days until the mice were sacrificed. For Ab anti-VLA4 administration, mice were, intraperitoneally, treated with 200 μg, every 4 days for three weeks. For each experiment, control mice were treated with the corresponding control IgG, with no differences between untreated wild type (wt) and IgG-treated wt mice.

2.3. Meningeal dissection

Mice were anesthetized with Zoletil and Rompun and were transcardially perfused with ice-cold PBS to remove circulating immune cells (Garofalo et al., 2023). To isolate the meninges, the skull cap was removed by performing two lateral incisions starting from the foramen magnum until the nasal bone. Meninges (mainly the dura layer (Merlini et al., 2022)) were detached from the skull and collected in Eppendorf vials containing 0.5 ml of DMEM.

2.4. Isolation of CD3−/NK1.1 + cells

The meninges and spleens of *C57BL/6* mice were enzymatically digested. The cell suspensions were washed and resuspended in staining buffer (PBS without Ca2+ Mg2+, BSA 0,5%, EDTA 2 mM and NaN3 0,025%), tagged with BD single cell multiplexing kit, mixed and stained with Zombie Violet for 15 min at room temperature for exclusion of dead cells and anti-CD16/32 blocking mAb (clone 24G2) for 10 min at 4 °C followed by incubation with anti-CD45, −CD3, −NK1.1 mAbs for 25 min. CD45+ CD3− NK1.1+ gated cells were sorted into PBS buffer 2% BSA 0,5 mM EDTA using a FACSAriaIII (BD Biosciences) equipped with a 488, 561 and a 633 nm laser and FACSDiva software (BD Biosciences version 6.1.3), and retained on ice. To reduce stress, cells were isolated in gentle FACS-sorting conditions using a ceramic nozzle of size 100 μm, a low sheath pressure of 19.84 lb-force per square inch (psi) that maintain the sample pressure at 18.96 psi and an acquisition rate of maximum 1500 events/s. FACS-sorted cells were confirmed to be 98% pure prior to RNA extraction. To evaluate intracellular markers, cells were fixed and permeabilized by using BD Cytofix/CytopermTM Fixation/Permeablization Kit. All cells were analyzed by flow cytometry using a FACSCanto II (BD Biosciences), and data were elaborated using FlowJo software (Becton Dickinson).

2.5. Single-cell transcriptomics

Cells from meninges and spleens were labeled using Single Cell Labeling with the BD Single-Cell Multiplexing Kit (BD Biosciences, # 633793). Briefly, cells were labeled with sample tags and each sample was washed twice with Stain buffer. Samples were counted in a hemocytometer (InCyto, DCH-NO1-5) staining the cells with Calcein AM (Thermo Fischer Scientific, #C1430) and Draq7TM (BD Biosciences, # 564904). Samples were pooled and resuspended in cold BD Sample Buffer (BD Biosciences) to achieve approximately 12.000 cells in 620 μL. Single cells from the pooled sample were isolated using Single Cell Capture and cDNA Synthesis with the BD Rhapsody Express Single-Cell Analysis System following the manufacturers protocol (BD Biosciences). After priming the nanowell cartridges, the pooled sample was loaded onto BD Rhapsody cartridge and incubated at room temperature. Cell Capture Beads (BD Biosciences) were prepared and then loaded onto the cartridge. According to the manufacturers protocol, cartridge was washed, cells were lysed, and Cell Capture Beads were retrieved and washed prior to performing reverse transcription and treatment with Exonuclease I. cDNA Libraries were prepared using mRNA whole transcriptome analysis (WTA) and Sample Tag library preparation protocol (BD Biosciences). The protocol allows to screen RNA expression of single cell using a 3′ WTA approach for samples that have been labeled with the BD Single-Cell Multiplexing Kit. PCR products were purified, and WTA mRNA PCR products were separated from sample tag products with double-sided size selection using AMPure XP magnetic beads (Beckman Coulter, # A63880). Quality and quantity of PCR products were determined by using an Agilent 2200 TapeStation with High Sensitivity D5000 ScreenTape (Agilent). Final libraries were indexed using PCR (9 or 6 cycles). Index PCR products were purified using SPRIselect magnetic beads. Quality of final libraries was assessed by using Agilent 2200 TapeStation with High Sensitivity D5000 ScreenTape and quantified using a Qubit Fluorometer using the Qubit dsDNA HS Kit (ThermoFisher, #Q32854). Final libraries were diluted to 4 nM and multiplexed for paired-end (2 × 75bp) sequencing on a NovaSe + q6000TM sequencer (Illumina). Sequence reads were aligned to the reference mouse genome mm10 (UCSC), following generation of barcode-gene matrices via the pipeline “BD Rhapsody™ WTA Analysis” from SevenBridges (https://www.sevenbridges.com/). The R package Seurat v4.05 was used under RStudio v4.1.5 for data trimming, unsupervised clustering and visualization according to the authors guidelines (Hao et al., 2021). In details, in order to remove poor quality cells, doublets and stressed cells, we excluded cells with a gene number less than 200, or

higher than the 93rd quantile. Mitochondrial gene ratio was calculated to filter out low quality cells (mitochondrial ratio ≥ 25%). Each experimental replicate was merged with the Seurat "integration" function (Stuart et al., 2019) and the resulting dataset was further processed with "SCTransform" for normalization and data scaling (Hafemeister and Satija, 2019). Highly variable genes (HVG, n = 3000) were also identified with the "SCTransform" function. The HVGs were used as input for principal component analysis (PCA). The first 30 PCAs were utilized in the subsequent analysis. With them, cells were, then, embedded by Umap plot with a resolution of 0.5. To assign cell identities, we applied the "FindAllMarkers" to identify differentially expressed genes (DEGs) among all genes by using Wilcoxon rank sum test.

We labelled NK cells as positive for the genes *Nkg7*, *Ncr1*, *Eomes*, *Klrg1*, *Cd27*, *Cd11b* and negative to *Cd3d* and *Cd3e*. ILC1 were considered if positive for *Tbx21*, *Cxcr6*, *Il7r* and *Xcl1*. The ssGSEA analysis on our scRNA dataset was performed with the "escape" package (v1.6.0) utilizing the murine gene sets "H", "C2", "C5", "C7" from the Molecular Signature Database (v7.4).

2.6. Surgical procedures

Adult male mice were implanted with plastic pedestals to record their EEG and EMG activities. They were anaesthetized with isoflurane (induction at 4% and sustained at 1–2%) and received a subcutaneous (s.c.) injection of buprenorphine (0.05 mg/kg). For EEG recordings, 4 SS electrodes with screws were implanted at the following coordinates from bregma: ground (AP = +2.0; ML = +2.5), reference (AP = -6.0; ML= +2.0), frontal cortex (AP= +2.8; ML = -0.5), parietal cortex (AP = -2.0; ML = -2.0). For EMG recordings, electrodes were inserted into the neck muscles. The implant was secured to the skull using dental acrylic (Decoeur et al., 2020; Nadjar et al., 2013). After surgery, mice were given one s.c. injection of carprofen (5 mg/kg). One-week post-surgery, mice were connected to the recording device for 1 day of habituation and their EEG/EMG data were recorded on the second day.

2.7. EEG/EMG experiments

The onset of the light phase was defined as Zeitgeber time (ZT) 0 (7:00 a.m.), and the onset of the dark phase as ZT12 (7:00p.m.), continuing until the next ZT0. For the NK cell-depleted group, mice were connected to the recording system for a 24-hour habituation period, followed by a 24-hour recording session. Animals were excluded from the study if they exhibited two or more signs of sickness behavior, including weight loss greater than 20%, reduced locomotion, hunched posture, piloerection, or seizures. Mice were also excluded if the wound surrounding the electrode implant site failed to heal properly.

EEG and EMG signals were acquired using Grass Technologies© 2011 (Twin software, version 4.5.3.23). Mice were tethered to an AS40 Amplifier system via a flexible cable. Signals were recorded at a sampling rate of 200 Hz and processed with an analog band-pass antialiasing filter. In consideration of the time-consuming procedure of analysis, the EEG–EMG analysis was limited from ZT5 to ZT12 in the light phase and from ZT17 to ZT0 in the dark phase.

Each video and EEG–EMG recording epoch lasting 8 s has been classified into the following behavioral classes:

1. *Active behavior* (movement condition). The mice performed overt movements in the cage for most of the given epoch of 8 s. The movements were characterized by ample displacements of body parts such as trunk, head, and forelimbs. Significant EMG activity was expected in this behavioral condition.
2. *Passive behavior (passive wake condition)*. The mice showed no movement (i.e., substantial immobility) periods intermingled with small movements of the trunk, head, and forelimbs for the majority of 8 s. The maximal duration of immobility considering two contiguous *epochs* was 8 s. This criterion was expected to minimize the risk that "passive condition" could be misclassified as sleep and vice–versa.
3. *Immobility condition.* The mice performed no movement of the trunk, head, and forelimbs for at least 20 s across three or more epochs. This condition was associated with a low EMG activity and required the analysis of the ongoing EEG and EMG waves for a discrimination *between* a condition of passive behavior and sleep (see below).

Afterward, the periods classified as "Immobility" were evaluated based on a standard visual analysis of EEG and EMG data. The classification of the animal immobility as non-rapid eye movement (NREM) sleep was based on the observation of sleep spindles (quite infrequent) and EEG slow sleep waves, whereas the classification as rapid eye movement (REM) sleep was based on the behavioral sleep state associated with low EMG activity and the following EEG features: dominant theta waves and no sleep spindles and EEG slow waves (Del Percio et al., 2017).

The NREM epochs between ZT21 and ZT0 were segmented offline into consecutive 4-second intervals. Any 4-second EEG segments containing muscular, EEG, electrocardiographic, instrumental, or other artifacts were identified by two independent experimenters and excluded. As previously described, EEG data were recorded using a monopolar montage with two recording electrodes implanted in the frontal and parietal cortex, and a reference electrode placed in the cerebellum. To minimize volume conduction effects, the EEG signals were re-referenced to a frontoparietal bipolar configuration by subtracting the parietal electrode signal from the frontal one. Spectral analysis was performed on EEG epochs re-referenced to this bipolar montage. Only artifact-free NREM epochs were used for the analysis of EEG delta power density, as a quantitative measure of sleep pressure (Decoeur et al., 2020; Halassa et al., 2009; Nadjar et al., 2013). This analysis was carried out using a standard Fast Fourier Transform (FFT) algorithm (Matlab; MathWorks, Natick, MA, USA), applying the Welch method with a Hanning window and a frequency resolution of 0.25 Hz, ranging from 0 to 40 Hz. For normalization, the value of each frequency bin was divided by the average value of all bins across the period under consideration for each mouse. This approach removed the original physical units of EEG power, resulting in an arbitrary scale where the normalized values reflect deviations from the two-hour average per frequency bin.

For XMG1.2 group, after the 24 h of habituation mice were analyzed during ZT10-ZT12 and ZT22-ZT0. For aVLA4 group and nNOScre mice, the analysis was conducted from ZT22 to ZT0.

2.8. Immunostaining

Mice were anesthetized and intracardially perfused with PBS and then 4% formaldehyde; brains were then isolated, fixed in 4% formaldehyde and snap frozen. Cryostat sections (20 μm) were washed in PBS, blocked (3% goat serum in 0.3% Triton X-100) for 1 h, at RT, and incubated overnight at 4 °C with specific antibodies diluted in PBS containing 1% goat serum and 0.1% Triton X-100. The sections were incubated with the following primary Abs: anti-c-fos 1:500 (Abcam Cat# ab208942; RRID:AB_2747772); anti-nNOS 1:200 (Abcam Cat# ab1376, RRID:AB_300614); anti-interferon-gamma receptor 1 1:100 (Thermo Fisher Scientific Cat# MA5-35147, RRID:AB_2849052) and anti-phosphoSTAT1 1:200 (Thermo Fisher Scientific Cat# 33–3400, RRID: AB_2533113). After several washes, sections were stained with the fluorophore-conjugated antibody and Hoechst (Cell Signaling Technology Cat# 4082, RRID:AB_10626776) for nuclei visualization and analyzed using a fluorescence microscope. For co-immunofluorescence, the secondary antibody was, subsequently, used. For all the antibodies staining, coronal sections were, first, boiled for 20 min in citrate buffer (pH 6.0) at 95–100°C. Images were digitized using a CoolSNAP camera (Photometrics, Tucson, USA) coupled to an ECLIPSE Ti-S microscope (Nikon, Tokyo, Japan). C-Fos and nNOS immunopositive neurons were counted manually using MetaMorph 7.6.5.0 image analysis software

(Molecular Device, San Jose, USA). c-Fos+ neurons were determined only when nuclear expression of c-Fos co-localized with Hoechst 33,342 staining. Interferon gamma receptor 1 and pSTAT1 immunopositive cells were measured the ratio of the area occupied by fluorescent cells versus the fluorescence of nNOS immunopositive cells (by converting pixels to square millimeters).

2.9. Fiber photometry and optogenetic cingulate cortex stimulation

nNOS^{cre} mice were anesthetized with Zoletil and Rompun for stereotaxic surgeries. For optogenetic stimulation, the virus (rAAV5-EF1α-DIO-hChR2-eYFP 500 nl) was injected into the cingulate cortex (AP: +1.4; ML: −0.5; DV: −1.4 from the dura) unilaterally, through a stainless steel 33-gauge internal cannula attached to a 10 μl Hamilton syringe, at a rate of 0.5 μl/min (5.8 μl total volume). After infusion, the cannula was kept at the injection site for 3 min and then slowly withdrawn. After 1 week, mice also received surgical implantation of a monofiber optic cannula (200 μm, 0.22NA, Ugo Basile), in the inoculation site. We used surgical sutures to close the skin, and mice were kept in a warm environment until resuming normal activity. Mice were allowed to recover for 2 weeks. Each cable was flexible so that mice could freely move about their cages.

In detail, mice were connected to fiber optic patch cords (Ugo Basile) using ceramic sleeves. Optogenetic stimulations (10 ms pulses at 1 Hz, 6 mW for 10 min, 10 ms pulses at 1 Hz, 12 mW for 10 min, 10 ms pulses at 1 Hz 19 mW for 10 min, 10 ms at 1 Hz 25 mW for 20 min and 10 ms pulses at 1 Hz, 0 mW for 10 min) were generated by a waveform generator (Intelligent optogenetics system, Ugo Basile, Italy) that triggered blue-light lasers (473 nm), for 3 s with 5-s cue light illumination and the house light off. The optogenetic stimulus cycle had been repeated for 2 times and during this period EEG and EMG analysis had been conducted.

2.10. Slice preparation for electrophysiology

Animals were decapitated under anesthesia with halothane and the whole brains were rapidly removed from the skull and immediately immersed in ice-cold sucrose-based artificial cerebrospinal fluid (aCSF; composition in mM: sucrose 63, NaCl 87, KCl 2, $CaCl_2$ 0.5, $MgCl_2$ 7, NaH_2PO_4 1.2, $NaHCO_3$ 25, glucose 10; 295–300 mOsm), continuously oxygenated with 95% O_2 and 5% CO_2 to maintain the proper pH (7.4). Coronal 300 μm slices were cut at 4°C with a vibratome (Thermo Scientific, USA) and then placed in a chamber containing oxygenated aCSF (composition in mM: NaCl 125, KCl 2, $CaCl_2$ 2, $MgCl_2$ 1.2, NaH_2PO^4 1.2, NaHCO3 25, glucose 10). After their preparation, slices were allowed to recover for at least 1 h at 30°C. Electrophysiological recordings were performed in the cingulate cortex.

2.11. Patch-clamp recordings

Slices were submerged in a recording chamber placed on the stage of an upright microscope (Leica DM-LFS) equipped with a water immersion 40 X objective (Leica) and a digital DCC camera (C8484, Hamamatsu) and visualized under infrared (IR) illumination. The preparation was continuously superfused (1–2 ml/min) with oxygenated aCSF at 34°C (TC324-C, Warner Instruments) by using a gravity-driven perfusion system. Whole-cell patch clamp recordings were performed from GFP-expressing nNOS + interneurons, visually identified under epifluorescence (Leica EL6000), by using a Multiclamp 700B amplifier (Molecular Devices, USA). Signals were acquired (sampling 10 kHz, low-pass filtered 2 kHz) with DigiData-1440A using pCLAMP-v10 software (Molecular Devices, USA). Borosilicate glass electrodes (3–4 MΩ) were pulled with a vertical puller (PC-10, Narishige). Pipette were filled with 110 mM K-Gluconate, 40 mM KCl, 10 mM Hepes, 0.2 mM EGTA, 3 mM Mg-ATP, 0.5 mM Na_2-GTP (295–300 mOsm, pH 7.2). Biocytin (0.2–0.4%; Tocris, 3349) was added freshly to the intracellular solution. After recordings, slices bearing neurons loaded with biocytin were fixed and stained for streptavidin to confirm the positivity for nNOS in the patched neurons. During recordings, cell capacitance was constantly monitored over the time and experiments where access resistance changed more than 20% were discarded. Resting Membrane Potential (RMP) was measured as the voltage with no injected current. Membrane capacitance was estimated as the total charge (i.e., the current integral, Qstep) mobilized in each cell by a 10 mV hyperpolarizing step (Vstep): Qstep/Vstep. The soma input was calculated as the slope of the linear fit of a I-V relationship measured in current clamp mode by 10 pA incremental current injection steps from −130 mV to −40 mV. Intrinsic excitability was examined by measuring the number of action potentials elicited from RMP by current injection steps (1 s of duration) incremented by 20 pA from 0 pA to 280 pA. Frequency-current relationship properties were calculated for the first instantaneous frequency (the reciprocal of the ISI between the first and the second AP) and the last instantaneous frequency (1/ISIlast). The firing pattern properties were evaluated at two times the rheobase calculating the instantaneous frequency as a function of interspike interval number. The properties of the action potential (AP) were measured from the first AP induced by a minimum suprathreshold current step, indicated as rheobase, applied to the cell from the RMP. The AP threshold is the value of the membrane potential at which a rapid upstroke of the AP starts (corresponding to the value of potential at which the action potential temporal derivative, dV/dt, crosses 10 V/s). The AP amplitude was measured as the voltage difference between the peak of the spike and the AP threshold. The AP duration is the spike width measured at its half-amplitude.

2.12. Statistics and reproducibility

Data are shown as the mean ± S.E.M. All the measurements were taken from distinct samples. Statistical significance was assessed by Student's *t* test, one-way ANOVA or two tails Student's *t* test for parametrical data, as indicated; Holm–Sidak test was used as a post-hoc test; Mann–Whitney Rank test and Wilcoxon matched pairs test for non-parametrical data. For multiple comparisons, multiplicity adjusted p-values are indicated in the corresponding figures. Statistical analyses comprising calculation of degrees of freedom were done using Sigma Plot 11.0, GraphPad Prism 9.0, Imaris 8 and Origin 7. For each experiment, the sample size (*n*) was chosen considering the following relation: $n \geq 2sigma\ (Zalpha/D)2$, where sigma is substituted by an estimate of variance (s2); alpha is at 0.05 (and Zalpha = − 2) and D is the difference among treatments. Criteria of animal exclusion/inclusion were pre-established; animals considered for the analysis were selected for age. At weaning, pups from different colonies were mixed and mice were randomly treated. The investigators performing the different analyses always received the samples from a third laboratory member, who was not involved in that specific experiment, to ensure blinding to the group allocation.

3. Results

3.1. NK cells mediate sleep pressure through cortical nNOS+ interneuron activation

To determine whether innate immunity contributes to sleep processes, we performed antibody-mediated depletion of NK1.1 INF-γ-producing cells, that in *C57BL/6* mice overlap with NK cells, ILC1 and NKT cells (Aibar et al., 2017) (Suppl. Fig. 1a), in mice exposed to 12:12 light/dark cycles (light: Zeitgeber Time [ZT] 0-ZT12, dark: ZT12-ZT24). The efficacy of depletion has been previously verified and the treatment did not lead to significant changes in other immune cell populations (Garofalo et al., 2023). NK1.1+ cell-depleted or control IgG-treated mice were analyzed for video, fronto-parietal EEG and back-muscle electromyography (EMG) recordings in 24 h. The absence of NK1.1+ cells induced a slower peak in the delta range compared with IgG-treated

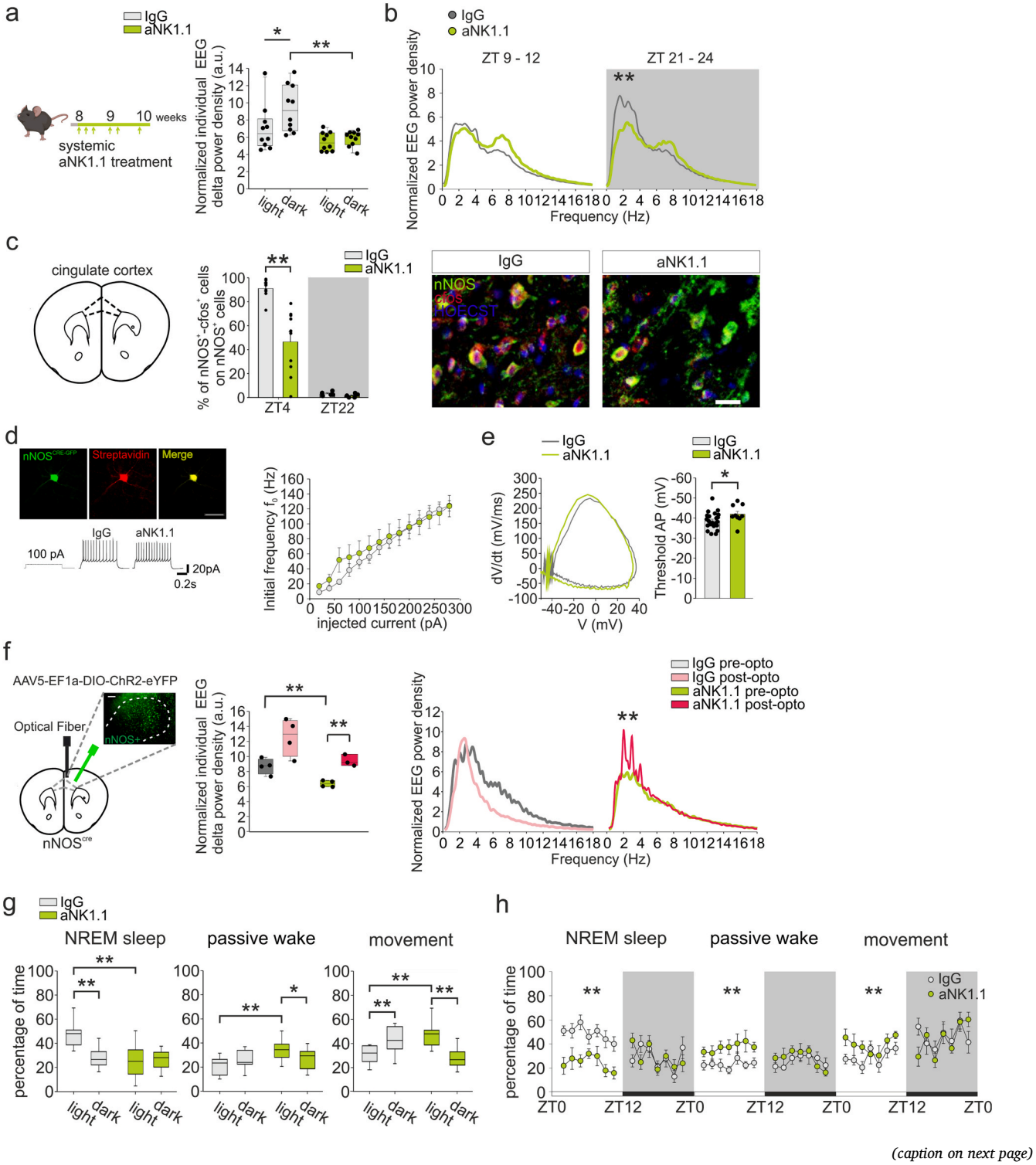

(caption on next page)

Fig. 1. NK cells depletion inhibits nNOS+ interneurons affecting sleep regulation. a) Left: Scheme of aNK1.1 treatment in *C57BL/6* mice. Normalized EEG power density in NREM sleep (arbitrary units a.u.) measured from ZT21 to ZT24 in IgG2a and aNK1.1 treated mice (n = 10 mice per condition * p = 0.0275 IgG2a mice light phase vs IgG2a mice dark phase; **p < 0.001 IgG2a vs aNK1.1 treated mice in dark phase, One-Way Anova test). b) Cumulative distribution of means of NREM sleep EEG delta power density in IgG2a and aNK1.1. (n = 10 mice per condition ** p < 0.001, One-Way Anova test). c) Percentage of nNOS+ -c-fos+ cells on nNOS+ cells in cingulate cortex of IgG2a and aNK1.1 treated mice at ZT22 and ZT4 (n = 10 mice per condition, 10 slices per animal 2 fields per slice ** p < 0.001, two-tails Student *t*-test). Data are expressed as mean ± SEM. The data variability reflects the very short and fragmented sleep period in mice, which makes it difficult to analyze during the same sleep phase in all animals. Representative immunofluorescences on the right. Scale bar: 20 μm. d) Representative pictures of recorded GFP+ nNOS+ interneurons stained with streptavidin (top) with example traces of AP trains evoked by 100pA current injection in IgG and aNK1.1 treated mice. The initial instantaneous firing frequency (f_o) measured between the first and second AP ($1/ISI_{1\text{-}2}$) of the spike train plotted vs. the injected current. e) Representative phase plot graphs for AP threshold detection (left) and histograms of mean AP threshold values in IgG2a and aNK1.1 treated mice with single dots indicating individual cell values (right) (n = 3 mice per condition, * p = 0.049, One-Way ANOVA test). f) Left: Representative scheme of virus injection and optic fiber implantation. Normalized EEG power density in NREM sleep (a.u.) measured from ZT21 to ZT24 in IgG2a and aNK1.1 treated mice before (pre-opto) and after (post-opto) optogenetic stimulation. Right: Representative distribution of NREM sleep EEG delta power density in IgG2a and aNK1.1 treated mice pre- and post- opto (n = 4 mice per condition, ** p = 0.001, One-Way ANOVA test). g) Mean time percentage spent in NREM Sleep (IgG2a in light vs IgG2a in dark phase ** p = 0.001 Wilcoxon matched-pairs signed rank test, IgG2a vs aNK1.1 in light phase ** p = 0.0007, Mann Whitney test), Passive Wake (aNK1.1 in dark phase versus aNK1.1 in light phase * p = 0.0166 Wilcoxon matched-pairs signed rank test, IgG2a vs aNK1.1 in light phase ** p = 0.008, Mann Whitney test) and Movement (IgG2a in light vs IgG2a in dark phase ** p = 0.0039, Wilcoxon matched-pairs signed rank test, IgG2a vs aNK1.1 in light phase p = 0.0003, Mann Whitney test, aNK1.1 in dark phase versus aNK1.1 in light phase ** p = 0.001 Wilcoxon matched-pairs signed rank test) by IgG2a and aNK1.1 treated mice (n = 10 mice per condition,). h) Cumulative distribution of the mean percentage of time spent in NREM Sleep (IgG2a vs aNK1.1 in light phase ** p = 0.0007, Mann Whitney test), Passive Wake (IgG2a vs aNK1.1 in light phase ** p = 0.008, Mann Whitney test) and Movement (IgG2a vs aNK1.1 in light phase **p = 0.0003, Mann Whitney test) by IgG2a and aNK1.1 treated mice from ZT5 to ZT11 and from ZT17 to ZT23 (n = 10 mice per condition,) For boxplots (a, f, g), the center line, boxes and whiskers represent the median, inner quartiles, and rest of the data distribution, respectively.

mice in the last part of dark phase (ZT21-24) (Fig. 1a, b), suggesting a deficit in the buildup of sleep needs. Since the SWA in NREM sleep results from the activation of GABAergic nNOS+ interneurons (Morairty et al., 2013; Pasumarthi et al., 2010) and considering that NK cells/ILC1 modulate the inhibitory transmission in the brain cortex through IFN-γ (Garofalo et al., 2023), we hypothesized that NK/ILC1 cells could modulate nNOS+ interneuron activity with impact on the sleep pressure. As expected, during the light phase (ZT4 as representative time point), we observed an increased activation of cortical nNOS+ interneurons in the cingulate cortex (evaluated with c-fos expression) (Fig. 1c) and NK1.1+ cells depletion reduced this effect (Fig. 1c). Moreover, patch clamp recording analysis revealed that NK1.1+ cell depletion does not alter the passive properties of these inhibitory neurons (Suppl. Fig. 1b, c), while influences the properties of their action potential, enhancing the threshold value, though without affecting the firing frequency (Fig. 1d, e; Suppl. Fig. 1d). This suggests an impact of NK1.1 cells on nNOS+ interneuron functioning. To test the contribution of NK1.1 cells to EEG delta power density in mice, we used an *in vivo* optogenetic strategy to control nNOS+ interneuron activity in freely moving mice (Fig. 1f). Optogenetic experiments were performed at ZT 22–24, when sleep pressure is typically increased and EEG showed a peak in delta power density. We took advantage of AAV ChR2:YFP to express the light-activated cation channel Channelrhodopsin2 in the nNOS+ interneurons of the cingulate cortex (Fig. 1f). The data shown in Fig. 1f demonstrated that optical activation of nNOS+ interneurons is sufficient to restore the spectral power in the lower-frequency range in NK1.1 cell-depleted mice in the dark phase, re-establishing the delta power similar to IgG-treated control mice. This provides one mechanistic link between innate immune cells and temporal regulation of cortical SWA. Video-EEG analysis showed that NK1.1 cell-depleted mice decrease the time spent sleeping (NREM sleep), and increase the passive wake time and movement, during the light phase (Fig. 1g, h; Suppl. Table 1), suggesting that the altered sleep pressure observed in the absence of NK1.1 cells at the end of the dark phase leads to a more active behavior during the light phase. No differences were observed in sleep behavior during the dark phase between aNK1.1- and IgG-treated mice (Fig. 1g, h).

3.2. Circadian rhythm of transcriptional landscape in meningeal and splenic NK cells

Meningeal NK cell-derived IFN-γ was recently associated with the regulation of cortical GABAergic activity (Filiano et al., 2016; Garofalo et al., 2023). To study the role of IFN-γ in regulating the sleep processes, we first investigated the possible circadian production of IFN-γ and other cytokines by CD3−/NK1.1+ NK cells and ILC1. To this aim, we studied the transcriptional landscape in meningeal or splenic NK cells and ILC1 of adult mice by single-cell RNA sequencing at ZT3 (light phase) and ZT22 (dark phase). We identified tissue specific populations of mature and immature NK cells between the spleen and the meninges, while we identified ILC1 cells only in the meninges (Fig. 2a, Suppl. Fig. 2a). The gene markers per cluster of cells are reported in Suppl. Table 2 and Suppl. Fig. 2b. We analyzed the differences between ZT3 and ZT22 (representative time points of light and dark phases respectively) NK and ILC1 pseudobulk populations in the expression of genes for cytokines, receptors or adhesion molecules, but we did not find any statistically significant difference (Fig. 2b; Suppl. Fig. 2a–f). Notably, we detected higher expression of *Ifng* transcripts in meningeal NK cells and ILC1, at both light and dark phases, compared to their splenic counterparts (Fig. 2c).

Then, we treated mice with natalizumab, an antibody directed against the integrin very-late antigen (VLA)-4 involved in lymphocyte extravasation (Gan et al., 2012; Yu et al., 2013), which efficiently reduced the number of meningeal NK1.1+ cells, with no effect of the number or frequency of peripheral cells (Garofalo et al., 2023, 2022). The efficiency of NK cell reduction in CNS after VLA-4 treatment in mice was already shown (Garofalo et al., 2023, 2022) (Suppl. Fig. 2g), and confirmed for these set of experiments. Natalizumab-treated mice showed a reduction in delta power peak at ZT22 (Fig. 2d, e), indicating a possible role of meningeal immunity in controlling sleep pressure, even if we cannot exclude the contribution of other CNS resident or peripheral immune cell populations (Garofalo et al., 2023; Korin et al., 2017).

3.3. Interferon-γ blockade impairs sleep pressure and alters NREM sleep

To explore the cellular target of NK1.1 cell-dependent IFN-γ on sleep, we verified the expression of IFN-γ receptor IFN-γR1 by nNOS+ interneurons in the cingulate cortex (Fig. 3a). The presence of IFN-γR in the mouse cortical neurons was already shown (Filiano et al., 2016), and we further validated the expression of ifngr1 gene in *C57BL/6* mouse brain using Allen Brain Atlas (Ifngr1 – RP_050503_02_D07 – sagittal). We then treated mice with XMG1.2, an IFN-γ blocking antibody (Garofalo et al., 2017) (see scheme in Fig. 3b), demonstrating that the IFN-γ blockade reduced the level of nNOS+ interneuron activation at ZT4 (Fig. 3b). The reduction of cfos+/nNOS+ interneurons runs parallel with a reduction of STAT1 phosphorylation (pSTAT) (Fig. 3c). This phosphorylation cascade is initiated when IFN-γ binds to its receptor, leading to the activation of JAK kinases which then phosphorylate

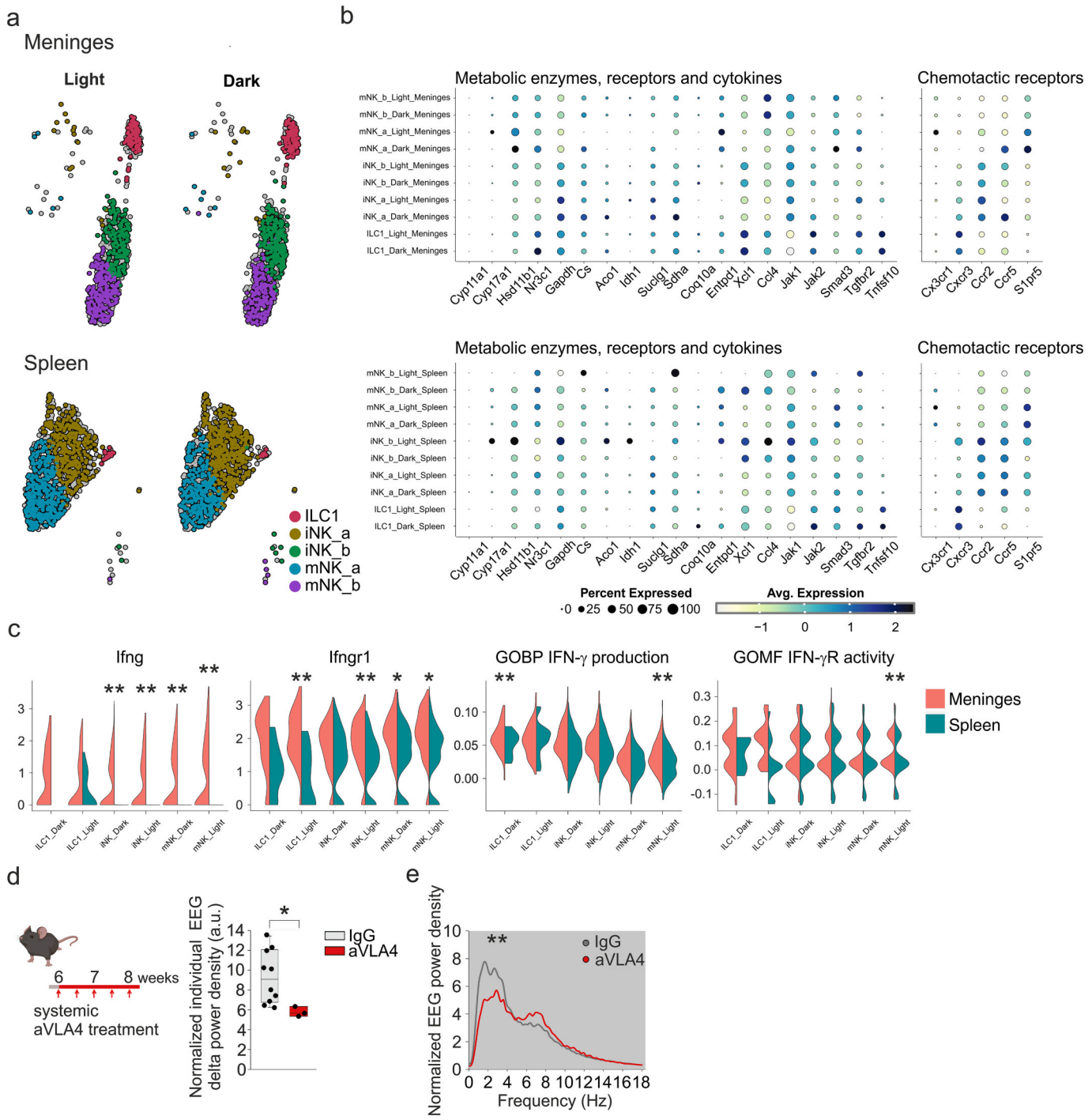

Fig. 2. Transcriptional landscape of meningeal and splenic NK/ILC1 cells at ZT3 and ZT15 a) Single cell RNA-sequencing of $CD3^{-}/NK1.1^{+}$ cells (n = 50 per time point, 2576 cells) derived from meninges and spleen at ZT3 and ZT15. b) Clusterization and expression level of metabolism-related genes and chemotactic receptors within the identified NK cells and ILC1 clusters in meninges and spleen at ZT3 and ZT15. c) Violin plots represent the distribution of IFN-γ, IFNγR1, and genes related to IFN-γ production and activity in meningeal and splenic subset of cells at ZT3 and ZT15 (* $p < 0.05$, ** $p < 0.01$, One-Way ANOVA test). d) Left: Scheme of aVLA4 treatment in *C57BL/6* mice. Normalized EEG power density in NREM sleep (a.u.) measured from ZT21 to ZT24 in IgG2a and aVLA4 treated mice (n = 10 IgG2a and n = 3 aVLA4, ** p = 0.008, One-Way ANOVA test). e) Cumulative distribution of individual NREM sleep EEG delta power density in IgG2a and aVLA4 treated mice (n = 10 IgG2a and n = 3 aVLA4 * p = 0.049 One-Way ANOVA test).

STAT1, suggesting an impairment in IFN-γR1 receptor activation. Similarly, aNK1.1 treatment reduced pSTAT1 in nNOS+ interneurons (Fig. 3c), strengthening the hypothesis of a link between NK1.1+ cells-IFN-γ-nNOS+ interneurons in sleep (ZT4). Consistently, XMG1.2-treated mice showed a reduction in the EEG delta power peak (Fig. 3d, e) and altered sleep behavior (Fig. 3f), similar to NK/ILC1 cell depleted mice (Fig. g, h). Altogether this evidence suggests that IFN-γ acts as a mediator that impacts the sleep process at steady state.

4. Discussion

The involvement of the immune system in the modulation of sleep processes under physiological conditions is still far from being fully understood. Current knowledge primarily indicates a bidirectional

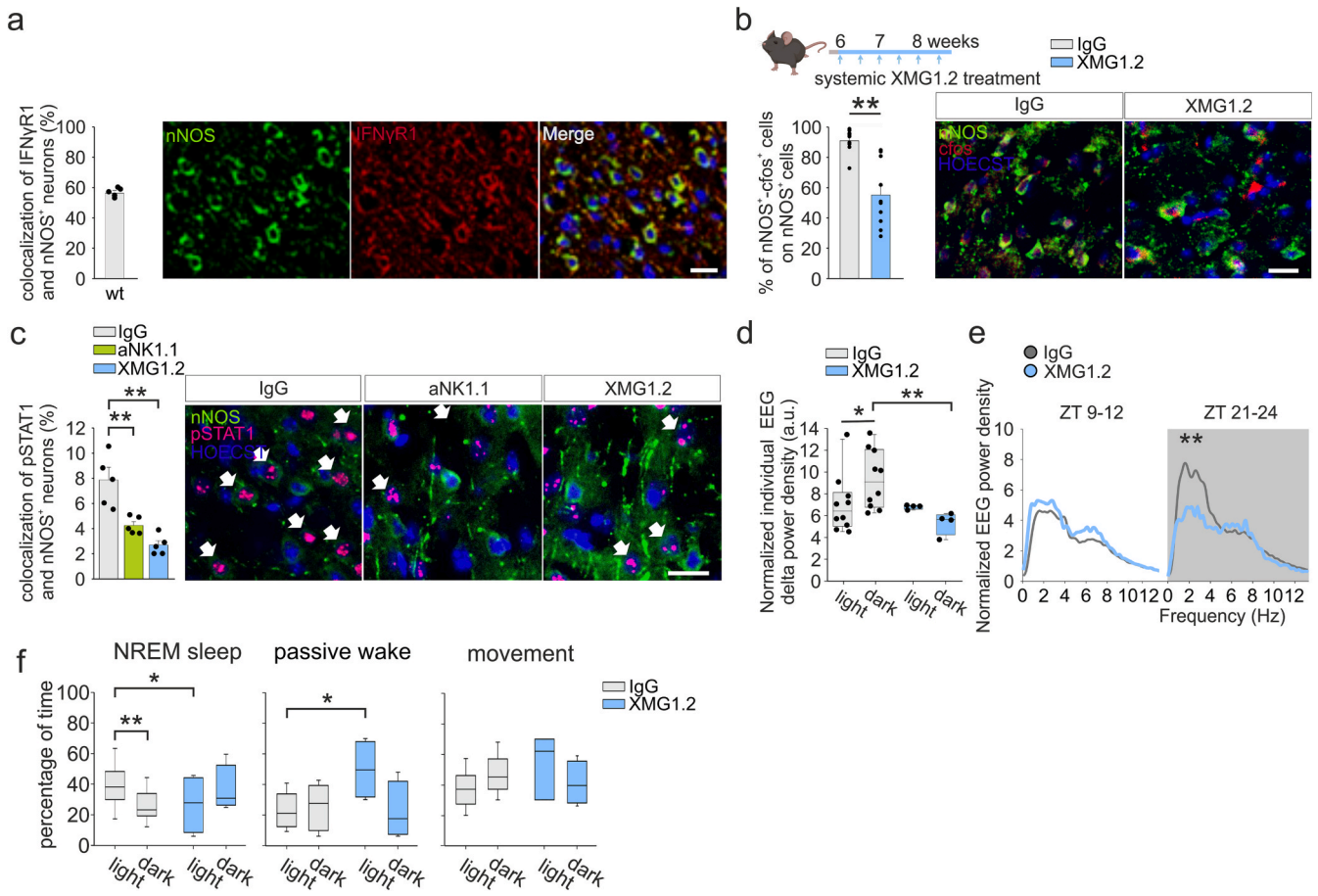

Fig. 3. Interferon gamma blockade mimics the effect of NK/ILC1 cell depletion in mice. a) Expression of IFNγR1 in the nNOS+ interneurons in cingulate cortex of wild type (wt) *C57BL/6* mice (n = 5). Representative immunofluorescences on the right. Data are expressed as mean ± SEM. Scale bar: 20 μm. b) Top: Scheme of XMG1.2 treatment in *C57BL/6* mice. Percentage of nNOS+ -c-fos+ cells on total nNOS+ cells in cingulate cortex of IgG2a and XMG1.2 treated mice at ZT4 (n = 10 mice per condition, ** $p < 0.001$ two-tails Student *t*-test). Data are expressed as mean ± SEM. The data variability reflects the very short and fragmented sleep period in mice, which makes it difficult to analyze during the same sleep phase in all animals. Representative immunofluorescences on the right. Scale bar: 20 μm. c) Percentage of nNOS+ -pSTAT1 + cells in cingulate cortex of IgG2a, aNK1.1 and XMG1.2 treated mice ZT4 (n = 5 mice per condition, ** $p = 0.008$ One-Way ANOVA test). Representative immunofluorescences on the right. Data are expressed as mean ± SEM. Scale bar: 20 μm. d) Normalized EEG power density in NREM sleep (a.u.) measured from ZT21 to ZT24 in IgG2a and XMG1.2 treated mice (n = 10 IgG2a and n = 4 XMG1.2, * $p = 0.0275$ ** $p = 0.003$, One-Way ANOVA test). e) Cumulative distribution of means of NREM sleep EEG delta power density in IgG2a and XMG1.2 treated mice (n = 10 IgG2a and n = 4 XMG1.2, ** $p = 0.005$, One-Way ANOVA test). f) Mean time percentage spent in NREM Sleep (IgG2a in light vs IgG2a in dark phase ** $p = 0.006$ One-Way ANOVA test, IgG2a vs aNK1.1 in light phase * $p = 0.025$, One-Way ANOVA test), Passive Wake (IgG2a vs aNK1.1 in light phase * $p = 0.018$, Mann Whitney test) and Movement (n = 10 mice per condition). Data are expressed as mean ± SEM. For boxplots (d, f) the center line, boxes and whiskers represent the median, inner quartiles, and rest of the data distribution, respectively. Summary of the NK/ILC1 cells- nNOS+ interneurons-sleep behavior axis in mice.

interaction between sleep and (innate and adaptive) immune functions and an important role of cortical nNOS+ inhibitory interneurons in generating NREM sleep (Besedovsky et al., 2019; Haspel et al., 2020; Irwin and Opp, 2017).

In this study, we use a multiscale approach to explore the involvement of the innate immune system and IFN-γ signaling in sleep processes in mice. Main findings unveil a causal role for NK1.1+ cells in maintaining the homeostatic activation of nNOS+ interneurons in the cingulate cortex during sleep, thereby modulating NREM-sleep and delta power as a measure of sleep pressure following extended wakefulness in the day light phase. These results are in line with previous evidence showing that IFN-γ shapes inhibitory tone and network synchrony in cortical circuits, suggesting a shared mechanism whereby this cytokine tunes the activity of GABAergic networks (Filiano et al., 2016). Parallel work in sleep neuroimmunology indicates that interferons interact with IL-1β, TNF-α, adenosine, and nitric oxide pathways to promote NREM sleep and slow-wave activity (Krueger et al., 2011). Within this framework, IFN-γ–dependent modulation of nNOS+ interneurons may represent a common pathway through which innate immune signals regulate circuit-level inhibition contributing to the build-up of slow-wave activity that underlies sleep pressure.

We propose the IFN-γ as a key soluble mediator that impacts sleep pressure. The circadian expression of IFN-γ was demonstrated in cultured splenic rat NK cells (Arjona et al., 2004; Arjona and Sarkar, 2005). At difference, our single cell RNA transcriptomic analysis did not unveil a different expression of IFN-γ or other cytokines at the light (ZT3) and dark (ZT22) phases in either meningeal or splenic ILC1 and NK cells isolated from mice. This difference could depend on the hours of the day selected for analyses, or on changes induced by *ex vivo* cell manipulation. However, we cannot exclude a diurnal rhythm of expression of IFN-γ receptor on cortical brain cell populations.

Since NK cells in *C57BL/6* mice largely overlap with ILC1 and NKT for the expression of the NK1.1 and NKp46 cell markers (Aibar et al., 2017), we should consider a possible role of these cell types in EEG delta activity modulation. However, the sequencing data suggest that meningeal NK cells and ILC1 are the major culprits since their exclusive production of IFN-γ.

We observed that IFN-γ modulated the activation of cortical nNOS+

interneurons in the cingulate cortex with effects on sleep pressure. However, the absence of neuronal-specific IFN-γR depletion limits the interpretation of nNOS+ interneurons as direct targets of IFN-γ activity in this mechanism. We cannot exclude that other brain resident cell populations, such as microglia or endothelial cells, which express high levels of IFN-γR (Kann et al., 2022; Ni et al., 2014), could mediate part of the phenotype.

Our results support the hypothesis of the role of meningeal immunity in the modulation of sleep pressure based on the following considerations: i) IFN-γ is only produced by meningeal NK cells and ILC1, compared to peripheral cells; ii) natalizumab treatment recapitulates the effects of NK1.1+ cell- and IFN-γ depletion. Additional experiments, such as intracerebral administration of aNK1.1 or localized manipulations, are necessary to establish the potential contribution of meninges and other IFN-γ −producing cells, such as CD8+ and CD4+ T cells in sleep, as well as to fully establish the role of meningeal immunity in sleep homeostasis (Filiano et al., 2016). Interestingly, it is conceivable that this mechanism of innate immune regulation of sleep may play a more prominent role in neonates, when T cells are not yet fully developed or functionally mature. In this context, innate lymphoid populations could compensate for the relative absence of adaptive T cell responses and contribute more substantially to early regulation of NREM sleep. Although this aspect was not directly addressed in our study, we agree that it represents an important area for future investigation, particularly in early-life settings.

The present study opens new avenues in understanding the contribution of innate immunity in sleep regulation during inflammatory diseases and the role of pro-inflammatory cytokines, including IL-1β, TNFα, and IFN-γ (Besedovsky et al., 2019; Imeri and Opp, 2009; Irwin and Opp, 2017; Jm et al., 2011). In addition our data suggest that sleep disturbance could represent a co-morbidity condition upon diseases where the activation of immune cells could hit the cortical inhibitory circuits, tuning the sleep pressure and the sleep behavior (Ehrenberg et al., 2018; Kashiwagi et al., 2024; Tsapanou et al., 2015). On the other hand, this raises the question of whether changes in NK cell/ILC1 activation indicate a primary pathology or a secondary consequence of disturbances in sleep.

In this context, additional physiological pathways may converge with IFN-γ signalling to influence sleep regulation. Sleep-dependent modulation of cerebrospinal fluid (CSF) flow and glymphatic exchange represents one such pathway, as NREM stages promote increased convective influx of CSF into the parenchyma, facilitating metabolic clearance and modulating cortical excitability (Chong et al., 2022). Further, ATP levels exhibit a sleep-dependent surge in wake-active cortical regions, tightly coupled to NREM delta power (Dworak et al., 2010). Prolonged wakefulness leads to extracellular adenosine accumulation, which promotes NREM sleep and slow-wave activity. These ATP–adenosine dynamics provide a biochemical substrate for sleep pressure and may operate alongside the IFN-γ–dependent modulation of nNOS+ interneurons.

Regardless, the association between immune alterations and disrupted sleep strengthens the rationale for targeting NK cells/ILC1 as a potential therapeutic strategy for sleep and neurological disturbance. As a limitation of this study, we acknowledge that our data do not establish a direct cause-effect relationship between the alteration of NREM-sleep EEG delta power in the NK1.1 cell-depleted mice and the reduction of sleep pressure and, in addition, we cannot exclude indirect mechanisms that modulate SWA, such as the alterations of the extracellular Cl^- concentration (Alfonsa et al., 2023) or the release of orexin (Garofalo et al., 2023).

In conclusion, we demonstrated that under physiological conditions, NK cells and ILC1 influence sleep pressure and the duration of sleep, disclosing also a key role for IFN-γ in the sleep–wake cycle.

We proposed that during the light phase, the cingulate cortex becomes responsive to the constitutive IFN-γ produced by NK cells leading to activation of nNOS+ interneurons, thereby promoting NREM sleep during the light period and enhancing sleep pressure and delta power buildup in the subsequent dark phase (Fig. 4).

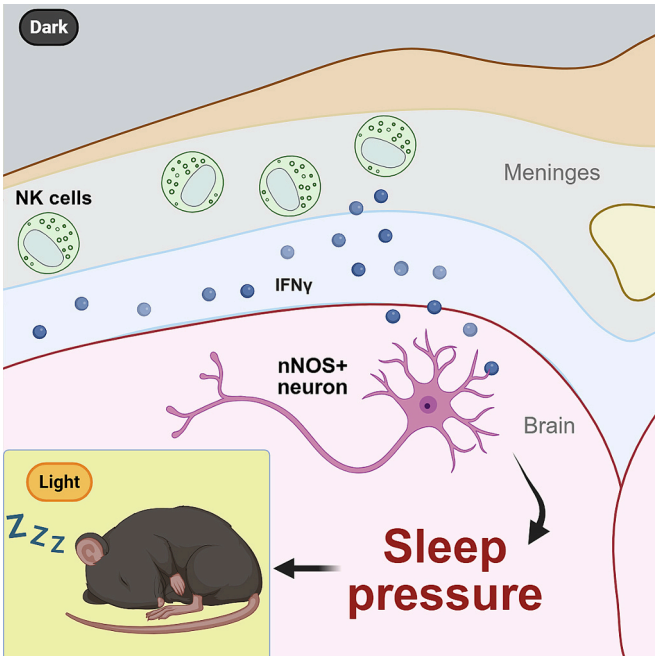

Fig. 4. Summary of the NK/ILC1 cells- nNOS+ interneurons-sleep behavior axis in mice.

CRediT authorship contribution statement

Alessandro Mormino: Writing – original draft, Methodology, Investigation, Data curation, Conceptualization. **Federico Tucci:** Writing – original draft, Methodology, Formal analysis, Data curation. **Germana Cocozza:** Formal analysis, Data curation. **Claudio Del Percio:** Formal analysis, Data curation. **Letizia Mazzarella:** Visualization, Investigation, Formal analysis. **Erika Di Pietro:** Methodology, Formal analysis, Data curation. **Maria Amalia Di Castro:** Methodology, Formal analysis, Data curation. **Giuseppina Chece:** Methodology. **Giovanni Bernardini:** Supervision. **Giuseppe Sciumè:** Supervision. **Giovanna Peruzzi:** Methodology. **Helena Stabile:** Methodology. **Cinzia Fionda:** Methodology. **Mattia Laffranchi:** Methodology, Formal analysis, Data curation. **Silvano Sozzani:** Supervision, Conceptualization. **Claudio Babiloni:** Writing – original draft, Supervision, Data curation, Conceptualization. **Cristina Limatola:** Writing – review & editing, Writing – original draft, Supervision, Funding acquisition, Conceptualization. **Stefano Garofalo:** Writing – review & editing, Writing – original draft, Supervision, Project administration, Methodology, Investigation, Funding acquisition, Formal analysis, Data curation, Conceptualization.

Funding

This work was supported by SG: NextGenerationEU DD.3175/2021 E DD.3138/2021 CN_3: National Center for Gene Therapy and Drugs based on RNA Technology Codice Progetto CN 00000041; RF GR-2021-12372494; PRIN 2022 2022488T5S; FIS Fondo Italiano per la Scienza FIS-2023-02628. CL: Italian Ministry of Universities and Research and by Progetto ECS 0000024 Rome Technopole-CUP B83C22002820006, PNRR Missione 4 Componente 2 Investimento 1.5, finanziato dall'Unione europea – NextGenerationEU; PRIN 2022 000126_2023_PRIN22_PNRR.

Declaration of competing interest

The authors declare that they have no known competing financial interests or personal relationships that could have appeared to influence the work reported in this paper.

Acknowledgments

We thank Dr. Matteo Carpi for his significant support in the present electroencephalographic data analysis.

Appendix A. Supplementary data

Supplementary data to this article can be found online at https://doi.org/10.1016/j.bbi.2026.106554.

Data availability

Data will be made available on request.

References

Aibar, S., González-Blas, C.B., Moerman, T., Huynh-Thu, V.A., Imrichova, H., Hulselmans, G., Rambow, F., Marine, J.-C., Geurts, P., Aerts, J., van den Oord, J., Atak, Z.K., Wouters, J., Aerts, S., 2017. SCENIC: single-cell regulatory network inference and clustering. Nat. Methods 14, 1083–1086. https://doi.org/10.1038/nmeth.4463.

Alfonsa, H., Burman, R.J., Brodersen, P.J.N., Newey, S.E., Mahfooz, K., Yamagata, T., Panayi, M.C., Bannerman, D.M., Vyazovskiy, V.V., Akerman, C.J., 2023. Intracellular chloride regulation mediates local sleep pressure in the cortex. Nat. Neurosci. 26, 64–78. https://doi.org/10.1038/s41593-022-01214-2.

Arjona, A., Boyadjieva, N., Sarkar, D.K., 2004. Circadian rhythms of granzyme B, perforin, IFN-gamma, and NK cell cytolytic activity in the spleen: effects of chronic ethanol. J. Immunol. 172, 2811–2817. https://doi.org/10.4049/jimmunol.172.5.2811.

Arjona, A., Sarkar, D.K., 2005. Circadian oscillations of clock genes, cytolytic factors, and cytokines in rat NK cells. J. Immunol. 174, 7618–7624. https://doi.org/10.4049/jimmunol.174.12.7618.

Besedovsky, L., Lange, T., Haack, M., 2019. The sleep-immune crosstalk in health and disease. Physiol. Rev. 99, 1325–1380. https://doi.org/10.1152/physrev.00010.2018.

Chong, P.L.H., Garic, D., Shen, M.D., Lundgaard, I., Schwichtenberg, A.J., 2022. Sleep, cerebrospinal fluid, and the glymphatic system: a systematic review. Sleep Med. Rev. 61, 101572. https://doi.org/10.1016/j.smrv.2021.101572.

Decoeur, F., Benmamar-Badel, A., Leyrolle, Q., Persillet, M., Layé, S., Nadjar, A., 2020. Dietary N-3 PUFA deficiency affects sleep-wake activity in basal condition and in response to an inflammatory challenge in mice. Brain Behav. Immun. Nutr. Immun. Mental Health 85, 162–169. https://doi.org/10.1016/j.bbi.2019.05.016.

Del Percio, C., Drinkenburg, W., Lopez, S., Infarinato, F., Bastlund, J.F., Laursen, B., Pedersen, J.T., Christensen, D.Z., Forloni, G., Frasca, A., Noè, F.M., Bentivoglio, M., Fabene, P.F., Bertini, G., Colavito, V., Kelley, J., Dix, S., Richardson, J.C., Babiloni, C., 2017. On-going electroencephalographic rhythms related to cortical arousal in wild-type mice: the effect of aging. Neurobiol. Aging 49, 20–30. https://doi.org/10.1016/j.neurobiolaging.2016.09.004.

Dworak, M., McCarley, R.W., Kim, T., Kalinchuk, A.V., Basheer, R., 2010. Sleep and brain energy levels: ATP changes during sleep. J. Neurosci. 30, 9007–9016. https://doi.org/10.1523/JNEUROSCI.1423-10.2010.

Ehrenberg, A.J., Suemoto, C.K., França Resende, E. de P., Petersen, C., Leite, R.E.P., Rodriguez, R.D., Ferretti-Rebustini, R.E. de L., You, M., Oh, J., Nitrini, R., Pasqualucci, C.A., Jacob-Filho, W., Kramer, J.H., Gatchel, J.R., Grinberg, L.T., 2018. Neuropathologic Correlates of Psychiatric Symptoms in Alzheimer's Disease. J Alzheimers Dis 66, 115–126. https://doi.org/10.3233/JAD-180688.

Filiano, A.J., Xu, Y., Tustison, N.J., Marsh, R.L., Baker, W., Smirnov, I., Overall, C.C., Gadani, S.P., Turner, S.D., Weng, Z., Peerzade, S.N., Chen, H., Lee, K.S., Scott, M.M., Beenhakker, M.P., Litvak, V., Kipnis, J., 2016. Unexpected role of interferon-γ in regulating neuronal connectivity and social behaviour. Nature 535, 425–429. https://doi.org/10.1038/nature18626.

Gan, Y., Liu, R., Wu, W., Bomprezzi, R., Shi, F.-D., 2012. Antibody to α4 integrin suppresses natural killer cells infiltration in central nervous system in experimental autoimmune encephalomyelitis. J. Neuroimmunol. 247, 9–15. https://doi.org/10.1016/j.jneuroim.2012.03.011.

Garofalo, S., Cocozza, G., Bernardini, G., Savage, J., Raspa, M., Aronica, E., Tremblay, M.-E., Ransohoff, R.M., Santoni, A., Limatola, C., 2022. Blocking immune cell infiltration of the central nervous system to tame Neuroinflammation in Amyotrophic lateral sclerosis. Brain Behav. Immun. 105, 1–14. https://doi.org/10.1016/j.bbi.2022.06.004.

Garofalo, S., Cocozza, G., Mormino, A., Bernardini, G., Russo, E., Ielpo, D., Andolina, D., Ventura, R., Martinello, K., Renzi, M., Fucile, S., Laffranchi, M., Mortari, E.P., Carsetti, R., Sciumè, G., Sozzani, S., Santoni, A., Tremblay, M.-E., Ransohoff, R.M., Limatola, C., 2023. Natural killer cells and innate lymphoid cells 1 tune anxiety-like behavior and memory in mice via interferon-γ and acetylcholine. Nat. Commun. 14, 3103. https://doi.org/10.1038/s41467-023-38899-3.

Garofalo, S., Porzia, A., Mainiero, F., Angelantonio, S.D., Cortese, B., Basilico, B., Pagani, F., Cignitti, G., Chece, G., Maggio, R., Tremblay, E., Savage, J., Bisht, K., Esposito, V., Bernardini, G., Seyfried, T., Mieczkowski, J., Stepniak, K., Kaminska, B., Santoni, A., Limatola, C., 2017. Environmental stimuli shape microglial plasticity in glioma [WWW Document]. eLife. https://doi.org/10.7554/eLife.33415.

Gerashchenko, D., Schmidt, M.A., Zielinski, M.R., Moore, M.E., Wisor, J.P., 2018. Sleep state dependence of optogenetically-evoked responses in neuronal nitric oxide synthase-positive cells of the cerebral cortex. Neuroscience 379, 189–201. https://doi.org/10.1016/j.neuroscience.2018.02.006.

Gerashchenko, D., Wisor, J.P., Burns, D., Reh, R.K., Shiromani, P.J., Sakurai, T., de la Iglesia, H.O., Kilduff, T.S., 2008. Identification of a population of sleep-active cerebral cortex neurons. Proc. Natl. Acad. Sci. 105, 10227–10232. https://doi.org/10.1073/pnas.0803125105.

Hafemeister, C., Satija, R., 2019. Normalization and variance stabilization of single-cell RNA-seq data using regularized negative binomial regression. Genome Biol. 20, 296. https://doi.org/10.1186/s13059-019-1874-1.

Halassa, M.M., Florian, C., Fellin, T., Munoz, J.R., Lee, S.-Y., Abel, T., Haydon, P.G., Frank, M.G., 2009. Astrocytic modulation of sleep homeostasis and cognitive consequences of sleep loss. Neuron 61, 213–219. https://doi.org/10.1016/j.neuron.2008.11.024.

Hao, Y., Hao, S., Andersen-Nissen, E., Mauck, W.M., Zheng, S., Butler, A., Lee, M.J., Wilk, A.J., Darby, C., Zager, M., Hoffman, P., Stoeckius, M., Papalexi, E., Mimitou, E. P., Jain, J., Srivastava, A., Stuart, T., Fleming, L.M., Yeung, B., Rogers, A.J., McElrath, J.M., Blish, C.A., Gottardo, R., Smibert, P., Satija, R., 2021. Integrated analysis of multimodal single-cell data. Cell 184, 3573–3587.e29. https://doi.org/10.1016/j.cell.2021.04.048.

Haspel, J.A., Anafi, R., Brown, M.K., Cermakian, N., Depner, C., Desplats, P., Gelman, A. E., Haack, M., Jelic, S., Kim, B.S., Laposky, A.D., Lee, Y.C., Mongodin, E., Prather, A. A., Prendergast, B.J., Reardon, C., Shaw, A.C., Sengupta, S., Szentirmai, É., Thakkar, M., Walker, W.E., Solt, L.A., 2020. Perfect timing: circadian rhythms, sleep, and immunity - an NIH workshop summary. JCI Insight 5 (e131487), 131487. https://doi.org/10.1172/jci.insight.131487.

Huber, R., Ghilardi, M.F., Massimini, M., Tononi, G., 2004. Local sleep and learning. Nature 430, 78–81. https://doi.org/10.1038/nature02663.

Imeri, L., Opp, M.R., 2009. How (and why) the immune system makes us sleep. Nat. Rev. Neurosci. 10, 199–210. https://doi.org/10.1038/nrn2576.

Irwin, M.R., Opp, M.R., 2017. Sleep health: reciprocal regulation of sleep and innate immunity. Neuropsychopharmacology 42, 129–155. https://doi.org/10.1038/npp.2016.148.

Jm, K., Jm, C., Bd, W., Mr, Z., P, T., Ka, J., Cj, D., 2011. Involvement of cytokines in slow wave sleep. Progress in brain research 193. https://doi.org/10.1016/B978-0-444-53839-0.00003-X.

Kann, O., Almouhanna, F., Chausse, B., 2022. Interferon γ: a master cytokine in microglia-mediated neural network dysfunction and neurodegeneration. Trends Neurosci. 45, 913–927. https://doi.org/10.1016/j.tins.2022.10.007.

Kashiwagi, M., Beck, G., Kanuka, M., Arai, Y., Tanaka, K., Tatsuzawa, C., Koga, Y., Saito, Y.C., Takagi, M., Oishi, Y., Sakaguchi, M., Baba, K., Ikuno, M., Yamakado, H., Takahashi, R., Yanagisawa, M., Murayama, S., Sakurai, T., Sakai, K., Nakagawa, Y., Watanabe, M., Mochizuki, H., Hayashi, Y., 2024. A pontine-medullary loop crucial for REM sleep and its deficit in Parkinson's disease. Cell 187, 6272–6289.e21. https://doi.org/10.1016/j.cell.2024.08.046.

Kattler, H., Dijk, D.J., Borbély, A.A., 1994. Effect of unilateral somatosensory stimulation prior to sleep on the sleep EEG in humans. J. Sleep Res. 3, 159–164. https://doi.org/10.1111/j.1365-2869.1994.tb00123.x.

Korin, B., Ben-Shaanan, T.L., Schiller, M., Dubovik, T., Azulay-Debby, H., Boshnak, N.T., Koren, T., Rolls, A., 2017. High-dimensional, single-cell characterization of the brain's immune compartment. Nat. Neurosci. 20, 1300–1309. https://doi.org/10.1038/nn.4610.

Krueger, J.M., Majde, J.A., Rector, D.M., 2011. Cytokines in immune function and sleep regulation. Handb. Clin. Neurol. 98, 229–240. https://doi.org/10.1016/B978-0-444-52006-7.00015-0.

Merlini, A., Haberl, M., Strauß, J., Hildebrand, L., Genc, N., Franz, J., Chilov, D., Alitalo, K., Flügel-Koch, C., Stadelmann, C., Flügel, A., Odoardi, F., 2022. Distinct roles of the meningeal layers in CNS autoimmunity. Nat. Neurosci. 25, 887–899. https://doi.org/10.1038/s41593-022-01108-3.

Morairty, S.R., Dittrich, L., Pasumarthi, R.K., Valladao, D., Heiss, J.E., Gerashchenko, D., Kilduff, T.S., 2013. A role for cortical nNOS/NK1 neurons in coupling homeostatic sleep drive to EEG slow wave activity. PNAS 110, 20272–20277. https://doi.org/10.1073/pnas.1314762110.

Nadjar, A., Blutstein, T., Aubert, A., Laye, S., Haydon, P.G., 2013. Astrocyte-derived adenosine modulates increased sleep pressure during inflammatory response. Glia 61, 724–731. https://doi.org/10.1002/glia.22465.

Ni, C., Wang, C., Zhang, J., Qu, L., Liu, X., Lu, Y., Yang, W., Deng, J., Lorenz, D., Gao, P., Meng, Q., Yan, X., Blasig, I.E., Qin, Z., 2014. Interferon-γ safeguards blood-brain barrier during experimental autoimmune encephalomyelitis. Am. J. Pathol. 184, 3308–3320. https://doi.org/10.1016/j.ajpath.2014.08.019.

Pasumarthi, R.K., Gerashchenko, D., Kilduff, T.S., 2010. Further characterization of sleep-active neuronal nitric oxide synthase neurons in the mouse brain. Neuroscience 169, 149–157. https://doi.org/10.1016/j.neuroscience.2010.04.066.

Sawada, T., Iino, Y., Yoshida, K., Okazaki, H., Nomura, S., Shimizu, C., Arima, T., Juichi, M., Zhou, S., Kurabayashi, N., Sakurai, T., Yagishita, S., Yanagisawa, M., Toyoizumi, T., Kasai, H., Shi, S., 2024. Prefrontal synaptic regulation of homeostatic

sleep pressure revealed through synaptic chemogenetics. Science 385, 1459–1465. https://doi.org/10.1126/science.adl3043.
Siclari, F., Tononi, G., 2017. Local aspects of sleep and wakefulness. Curr. Opin. Neurobiol. 44, 222–227. https://doi.org/10.1016/j.conb.2017.05.008.
Stuart, T., Butler, A., Hoffman, P., Hafemeister, C., Papalexi, E., Mauck, W.M., Hao, Y., Stoeckius, M., Smibert, P., Satija, R., 2019. Comprehensive integration of single-cell data. Cell 177, 1888–1902.e21. https://doi.org/10.1016/j.cell.2019.05.031.
Thomas, C.W., Guillaumin, M.C., McKillop, L.E., Achermann, P., Vyazovskiy, V.V., 2020. Global sleep homeostasis reflects temporally and spatially integrated local cortical neuronal activity. eLife 9, e54148. https://doi.org/10.7554/eLife.54148.
Tsapanou, A., Gu, Y., Manly, J., Schupf, N., Tang, M.-X., Zimmerman, M., Scarmeas, N., Stern, Y., 2015. Daytime sleepiness and sleep inadequacy as risk factors for dementia. Dement Geriatr Cogn Dis Extra 5, 286–295. https://doi.org/10.1159/000431311.
Vyazovskiy, V.V., Welker, E., Fritschy, J.-M., Tobler, I., 2004. Regional pattern of metabolic activation is reflected in the sleep EEG after sleep deprivation combined with unilateral whisker stimulation in mice. Eur. J. Neurosci. 20, 1363–1370. https://doi.org/10.1111/j.1460-9568.2004.03583.x.
Yu, Y., Schürpf, T., Springer, T.A., 2013. How natalizumab binds and antagonizes α4 integrins*. J. Biol. Chem. 288, 32314–32325. https://doi.org/10.1074/jbc.M113.501668.
Zielinski, M.R., Atochin, D.N., McNally, J.M., McKenna, J.T., Huang, P.L., Strecker, R.E., Gerashchenko, D., 2019. Somatostatin+/nNOS+ neurons are involved in delta electroencephalogram activity and cortical-dependent recognition memory. Sleep 42, zsz143. https://doi.org/10.1093/sleep/zsz143.